

Fast cold gas in hot AGN outflows

Tiago Costa^{*}, Debora Sijacki and Martin G. Haehnelt

Institute of Astronomy and Kavli Institute for Cosmology, University of Cambridge, Madingley Road, Cambridge CB3 0HA, UK

5 October 2018

ABSTRACT

Observations of the emission from spatially extended cold gas around bright high-redshift QSOs reveal surprisingly large velocity widths exceeding 2000 km s^{-1} , out to projected distances as large as 30 kpc. The high velocity widths have been interpreted as the signature of powerful AGN-driven outflows. Naively, these findings appear in tension with hydrodynamic models in which AGN-driven outflows are energy-driven and thus very hot with typical temperatures $T \gtrsim 10^{6-7} \text{ K}$. Using the moving-mesh code AREPO, we perform ‘zoom-in’ cosmological simulations of a $z \sim 6$ QSO and its environment, following black hole growth and feedback via energy-driven outflows. In the simulations, the QSO host galaxy is surrounded by a clumpy circum-galactic medium pre-enriched with metals due to supernovae-driven galactic outflows. As a result, part of the AGN-driven hot outflowing gas can cool radiatively, leading to large amounts ($\gtrsim 10^9 M_{\odot}$) of cold gas comoving with the hot bipolar outflow. This results in velocity widths of spatially extended cold gas similar to those observed. We caution, however, that gas inflows, random motions in the deep potential well of the QSO host galaxy and cooling of supernovae-driven winds contribute significantly to the large velocity width of the cold gas in the simulations, complicating the interpretation of observational data.

Key words: methods: numerical - cosmology: theory - quasars: supermassive black holes

1 INTRODUCTION

Bright quasars (QSOs) with luminosities $L \gtrsim 10^{47} \text{ erg s}^{-1}$ powered by supermassive black holes with masses $\gtrsim 10^9 M_{\odot}$ exist already at $z = 6 - 7$ (Fan et al. 2001; Willott et al. 2007; Mortlock et al. 2011; De Rosa et al. 2014). Their extreme luminosities are thought to be generated via gravitational accretion of baryonic material onto the black hole (Lynden-Bell 1969; Rees 1984). It has been repeatedly argued that it only takes a small fraction of the emitted energy to couple with its host galaxy to unbind it entirely (Silk & Rees 1998; Haehnelt et al. 1998; King 2003; Fabian 2012). Such feedback from AGN has been identified as an important process in the evolution of galaxies due to its promise in facilitating the observed rapid quenching of star formation in massive galaxies (Scannapieco & Oh 2004; Springel et al. 2005b; Croton et al. 2006; Bower et al. 2006; Dubois et al. 2013; Sijacki et al. 2014).

Energy and/or momentum deposition by AGN is certainly capable of launching powerful outflows extending to galactic scales of tens of kpc in high-redshift QSOs (e.g. Costa et al. 2014a,b). Whether the coupling of energy and/or momentum to the ISM occurs (magneto-)hydrodynamically

via the shocking of a fast inner wind or via direct radiation pressure is, however, intensely debated. The inferred momentum flux in observed outflows often appears to exceed the momentum flux L/c of the AGN radiation field (e.g. Sturm et al. 2011; Cicone et al. 2014a; Genzel et al. 2014). Here, we assume that the wind is driven hydrodynamically. In this picture, the observed momentum fluxes $> L/c$ favour an ‘energy-driven’ wind over a ‘momentum-driven’ model (Zubovas & Nayakshin 2012; Faucher-Giguère & Quataert 2012; Nayakshin 2014; Costa et al. 2014b).

One of the potential challenges to energy-driven outflow models is their prediction that the outflow is not only fast, but also hot and tenuous. Observations, however, suggest that a significant component of AGN-driven outflows is cold and dense molecular gas (e.g. Aalto et al. 2012; Cicone et al. 2014a). It has been argued that, in the absence of magnetic fields, the hot outflow is unable to fully drag cold gas by ram pressure without disrupting it (see e.g. McCourt et al. 2014). A possible route to a cold component in hot energy-driven outflows is instead radiative cooling of the shocked swept-up material (Zubovas & King 2014). In this Letter, we investigate whether the cooling of hot energy-driven outflows in cosmological simulations of a bright QSO at $z \sim 6$ can account for a cold outflowing component. We compare our predictions for the spatial distribution and kinematics of the

^{*} E-mail: taf34@ast.cam.ac.uk

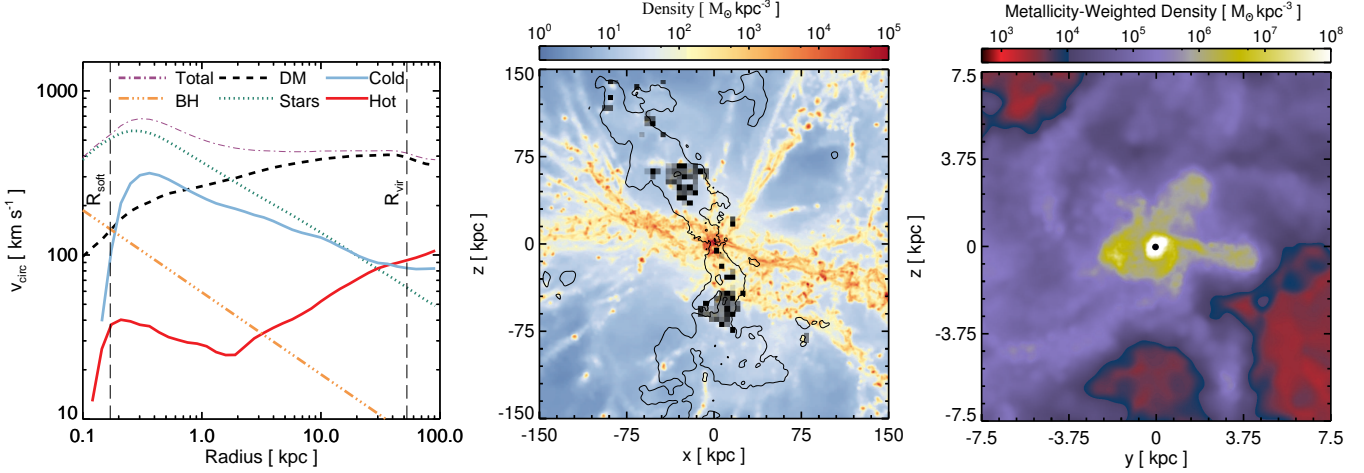


Figure 1. **Left:** Circular velocity ($v_{\text{circ}} = \sqrt{GM(<r)/r}$) of dark matter, hot and cold gas, stars and the central black hole of the QSO host halo in the simulation with both supernovae and AGN feedback at $z = 6.6$. Vertical lines show the location of the gas softening length (R_{soft}) and the virial radius of the host halo (R_{vir}). **Middle:** Gas density projected along a slab with thickness 300 kpc at $z = 6.6$. The contour shows the hot component of the outflow with a velocity of 500 km s^{-1} . The location and radial velocity-weighted mass of outflowing cold clouds is marked with pixels, with darker colours indicating a higher mass in the cold phase. **Right:** Zoom-in into the central 15 kpc of the QSO host galaxy showing metallicity-weighted gas density. The remarkably compact central disc is oriented perpendicularly to the large-scale outflow and is fed by a system of cold gas filaments. The location of the most massive black hole ($M_{\text{BH}} = 8.2 \times 10^8 M_{\odot}$) is marked with a black circle.

cold gas with the recent interferometric PdBI observations of an AGN-driven cold outflow detected in a luminous $z \approx 6.4$ QSO (Cicone et al. 2015).

2 NUMERICAL SIMULATIONS

We employ the moving-mesh code AREPO (Springel 2010) in order to follow the hydrodynamics of the cosmic gas component, treated as an ideal inviscid fluid. We include radiative primordial cooling as modelled in Katz et al. (1996) combined with metal-line cooling as treated in Vogelsberger et al. (2013). We also include heating due to a spatially uniform time-dependent UV background (Faucher-Giguère et al. 2009). Our simulation suite consists of ‘zoom-in’ resimulations of the six most massive haloes found in the Millennium volume (Springel et al. 2005a) at $z = 6.2$ and captures the likely cosmological sites of the brightest high redshift QSOs (Sijacki et al. 2009; Costa et al. 2014a)^{*}. In order to model energy-driven outflows, we adopt the prescription described in Costa et al. (2014b), which successfully recovers the analytical wind solution for energy-driven shells. Note that we now follow black hole accretion self-consistently as in Costa et al. (2014a). We also investigate simulations with supernovae-driven outflows (Springel & Hernquist (2003), see also Costa et al. (2014a)). In this Letter, we isolate the effects of feedback by analysing four different runs: 1. simulation without supernovae or AGN feedback (No Feedback), 2. simulation with supernovae-driven winds with mass loading

$\eta = 1$ and velocity 1183 km s^{-1} comparable with the escape speed from the AGN host halo (SN Feedback), 3. simulation with energy-driven AGN winds (AGN Feedback), and 4. simulation with combined supernovae- and AGN-driven outflows (SN+AGN Feedback). To distinguish different gas phases, we consider a temperature cut of $\geq 10^6 \text{ K}$ for ‘hot gas’ and $\leq 5 \times 10^4 \text{ K}$ for ‘cold gas’ additionally including ‘star-forming’ gas lying along the ISM effective equation of state[†]. Since most of the gas at temperatures $\leq 5 \times 10^4 \text{ K}$ has cooled to the temperature floor of 10^4 K , our results are only mildly sensitive to this definition. All spatial coordinates are given in physical units.

3 RESULTS

At $z = 6.6$, the simulated QSO has a bolometric luminosity of $L_{\text{bol}} \approx 10^{47} \text{ erg s}^{-1}$ powered by a black hole of mass $M_{\text{BH}} = 8.2 \times 10^8 M_{\odot}$ and hence has an Eddington ratio $\lambda_{\text{Edd}} = \dot{M}_{\text{BH}}/\dot{M}_{\text{Edd}} \approx 1$, all in line with observed properties of $z \gtrsim 6$ QSOs (e.g. De Rosa et al. 2014). In our simulations, the bright QSO is located in a very massive halo with $M_{\text{halo}} \approx 3 \times 10^{12} M_{\odot}$ within a tightly bound galaxy with a gaseous disc and a very compact flattened stellar bulge. The galaxy has a stellar mass of $2.2 \times 10^{10} M_{\odot}$ within a radius $\approx 0.3 \text{ kpc}$ and is undergoing a starburst with a total star formation rate of $\approx 470 M_{\odot} \text{ yr}^{-1}$. Note that star formation rates inferred from (sub)millimeter observations of high redshift QSO hosts can be even higher, reaching up to $3000 M_{\odot} \text{ yr}^{-1}$ (e.g. Bertoldi et al. 2003). The QSO host halo has a circular velocity $v_{\text{circ}} \approx 400 \text{ km s}^{-1}$ at the virial radius $R_{\text{vir}} \approx 53 \text{ kpc}$ (see Fig. 1) and is continuously

^{*} As discussed in Costa et al. (2014a), the volume probed by the Millennium simulation is still a factor ≈ 100 smaller than that probed by surveys of high-redshift QSOs. The host haloes should be even more massive than those considered in our simulations if the duty cycle is close to unity.

[†] We take the ‘cold gas’ in our simulations as proxy for molecular gas, which cannot be distinguished in our simulations due to unavoidable lack of resolution.

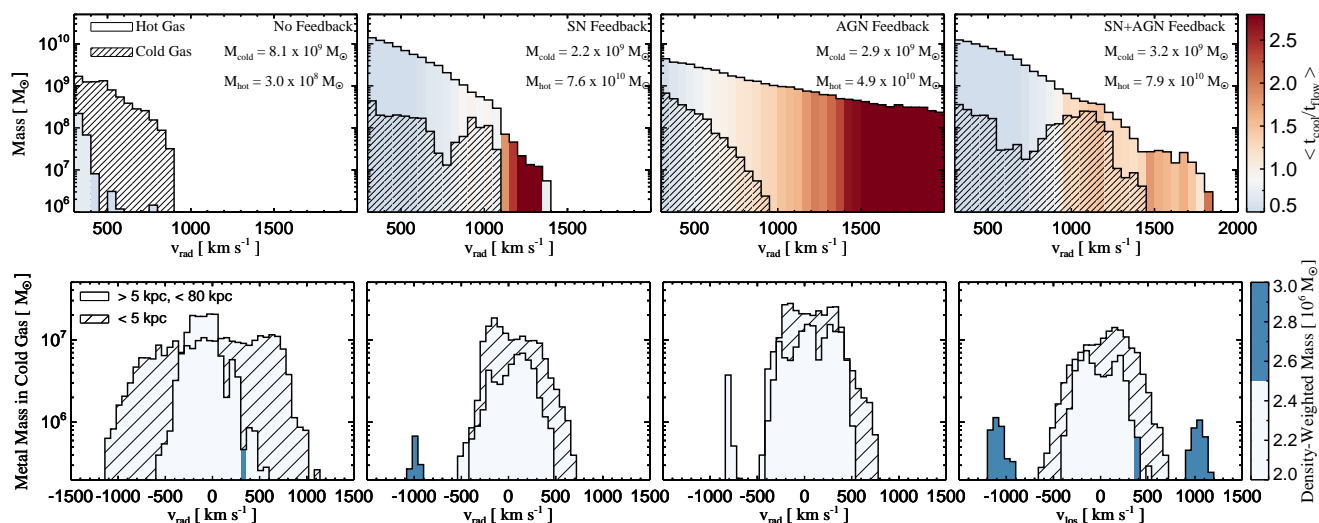


Figure 2. **Top row:** Cold gas mass per radial velocity bin within a sphere of radius 300 kpc centred on the QSO host galaxy. Bins are colour-coded according to the average ratio of cooling to flow time for the hot component $\langle t_{\text{cool}}/t_{\text{flow}} \rangle$. Cold comoving gas forms whenever the flow time becomes comparable to the cooling time. This occurs for gas of speeds of up to 1500 km s⁻¹ in simulation SN+AGN Feedback. A large amount of gas travels at faster speeds but does not cool sufficiently quickly and remains hot. The mass in cold and hot gas flowing out at speeds higher than 300 km s⁻¹ is labelled in each plot. Note that due to different black hole growth histories in simulations with different feedback, an AGN-driven outflow shown here only occurs at a slightly lower redshift of 6.3 in simulation AGN Feedback. **Bottom row:** Metal-enriched cold gas mass per line-of-sight velocity bin shown within radii 5 kpc (shaded) and between 5 and 80 kpc (coloured) at $z = 6.6$ ($z = 6.3$ in the AGN Feedback run). The line-of-sight was chosen to be perpendicular to the central gas disc. Colours give the density-weighted average mass in each bin. High gas speeds occur without any feedback, but all the fast moving gas is concentrated in the central regions of the halo. In order to produce spatially extended high velocity cold gas, strong outflows are required.

fed by three massive cold filaments, leading to the formation of the central bulge with a maximum circular velocity $v_{\text{circ}} \approx 700 \text{ km s}^{-1}$.

As previously reported, energy and momentum injection in the QSO host galaxy via star formation and black hole accretion leads to powerful galactic outflows in our simulations (Costa et al. 2014a). We here investigate whether the initially hot outflows are able to cool radiatively. In order for the outflow to cool, the flow time r/v_{rad} must exceed the cooling time $u_{\text{int}}/(n_{\text{H}}^2 \Lambda)$ of the shocked swept-up material. The histograms displayed in the top row of Fig. 2 show the distribution of radial velocities for hot (coloured) and cold (line-filled) gas for our four simulations. Due to the depth of the central potential well, positive radial velocities of up to $\approx 900 \text{ km s}^{-1}$ occur without either AGN or supernovae feedback, while the distribution of radially outflowing hot gas extends to $\approx 800 \text{ km s}^{-1}$. The subsequent panels in the top row show that a hot outflowing wind with velocities up to $\approx 1400 \text{ km s}^{-1}$ is launched in the simulation with supernovae feedback only, while the simulation with AGN feedback produces much faster hot outflows with velocities well beyond 2000 km s^{-1} .

The histograms are colour-coded according to the bin-averaged ratio of cooling time to flow time $\langle t_{\text{cool}}/t_{\text{flow}} \rangle$ of the hot component. The red tail of the histogram for gas with velocities $> 1500 \text{ km s}^{-1}$ in the simulations with AGN feedback and with both AGN and supernovae feedback represents gas with $\langle t_{\text{cool}}/t_{\text{flow}} \rangle \approx 1 - 3$. This ultrafast component of the hot gas cannot cool in the outflow. However, for somewhat slower gas, $\langle t_{\text{cool}}/t_{\text{flow}} \rangle \approx 1$ despite the still rather high speeds ($v_{\text{rad}} \lesssim 1300 \text{ km s}^{-1}$). In the simulation with supernovae feedback, a large fraction of the hot out-

flow can actually cool, leading to a significant enhancement of the amount of cold gas with radial velocities in the range $500 - 1100 \text{ km s}^{-1}$. It is, however, the combined effect of supernovae and AGN feedback that leads to the largest mass of fast ($\gtrsim 1000 \text{ km s}^{-1}$) outflowing cold gas and the highest outflow speeds ($\approx 1400 \text{ km s}^{-1}$). Note that in all simulations, the total mass of cold gas flowing out with speeds $v_{\text{rad}} > 300 \text{ km s}^{-1}$ exceeds $10^9 M_{\odot}$. Note that we verified that additional Compton heating from the QSO does not produce a significant effect over a flow time at radii of tens of kpc (e.g. Costa et al. 2014b).

In the bottom row of Fig. 2, we show the mass of metal-enriched cold gas as a function of 1D (line-of-sight) velocity along the pole of the QSO host galaxy. In the No Feedback simulation, all of the rapidly moving cold gas is located within the innermost 5 kpc of the halo. The potential well of the QSO host is so deep (see Fig. 1) that gravitational motions alone produce a velocity width for the cold gas[‡] of about 2000 km s^{-1} within a radius of 5 kpc. In simulations SN Feedback and AGN Feedback, the outflows clear out part of the gas in the central region of the galaxy, thus reducing the total mass in cold gas. The velocity widths of the cold gas are also somewhat smaller.

The combined effect of supernovae and AGN feedback has, however, a much larger effect on the spatial and velocity distribution of the cold gas. The supernovae-driven outflows lead to a more metal-enriched clumpy environment around the host galaxy which drives much more efficient

[‡] Note that in the absence of feedback processes, gas may become unrealistically compact.

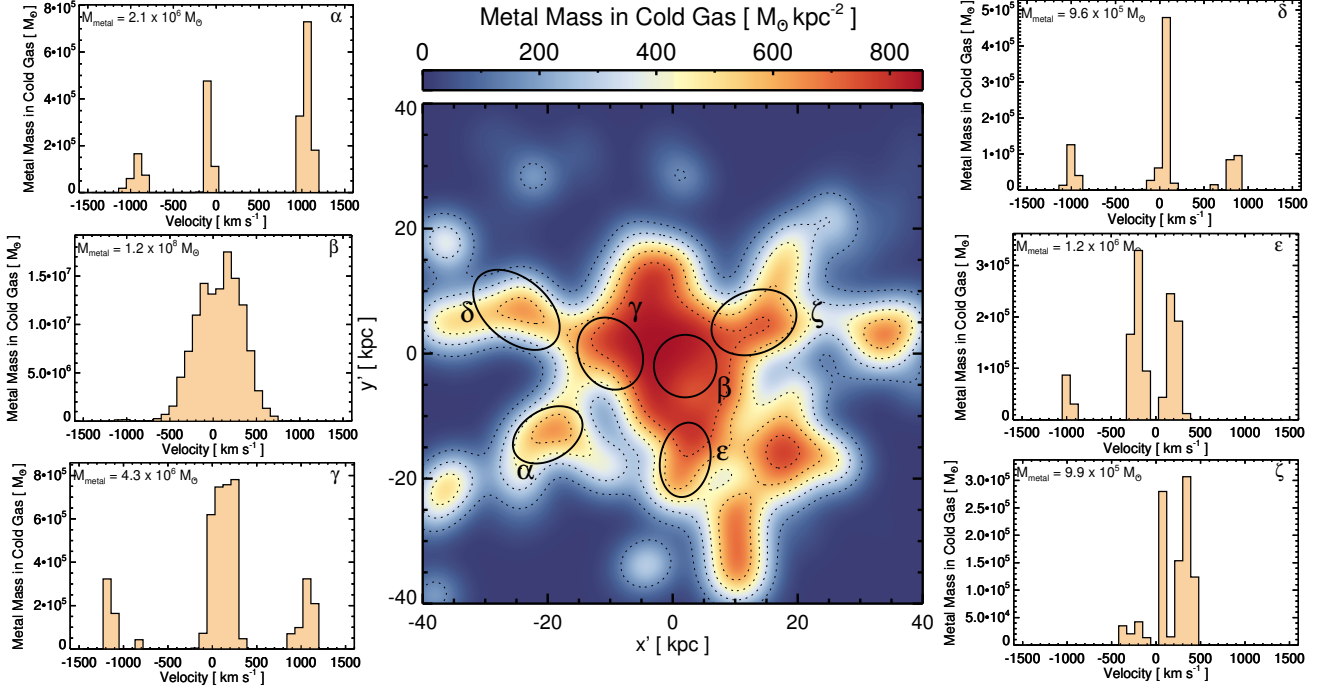


Figure 3. Cold gas mass in metals projected along the simulation volume and convolved with a Gaussian filter with FWHM of 6.7 kpc to match the resolution of observations by Cicone et al. (2015). Cold outflowing gas is spatially extended out to (projected) distances of 20 – 30 kpc and is characterised by a clumpy and very irregular morphology. The kinematics of the outflowing cold gas is illustrated by spectra extracted from various regions of the image. The individual spectra differ substantially from region to region and can be characterised by red and blue ‘wings’ symmetric in velocity space, tracing gas flowing out at speeds up to 1200 km s^{-1} or by a narrow component tracing low velocity gas. The narrow component is also spatially extended.

cooling within the AGN-driven fast hot outflow. As a result, the velocity width of the cold gas between radii of 5 and 80 kpc increases to $\approx 2400 \text{ km s}^{-1}$. The momentum flux of the cold gas embedded in the energy-driven outflow in our simulations is relatively low ($\approx 0.27L/c$) comparable to the $1.00 \pm 0.14L/c$ inferred by Cicone et al. (2015). The hot outflow driven by the AGN nevertheless contains a momentum flux of $\approx 3.3L/c$.

The central panel of Fig. 1 pictures the hot and cold outflows launched in the simulation with both supernovae and AGN feedback. The hot outflow takes paths of least resistance (see also Zubovas & Nayakshin 2012; Costa et al. 2014b) and propagates along the poles of the host galaxy (shown in the right panel), thereby avoiding regions of filamentary infall. The clumpier pockets of cold gas largely retain the geometry of the hot outflow from which they cooled and are spatially extended with radial distances up to $\approx 100 \text{ kpc}$ from the QSO.

Due to the anisotropy of the outflow, a spatial offset between the blue and red spectral wings is expected for most outflow orientations. For a bipolar outflow like that in our simulation, a spatial overlap between the red and blue wings of the velocity distribution requires a rather special orientation in which the line of sight is parallel to the symmetry axis of the outflow. The recent [CII] observations (Maiolino et al. 2012; Cicone et al. 2015) of the bright $z \approx 6.4$ QSO J1148+5152 show extremely broad wings extending to speeds of $\approx 1400 \text{ km s}^{-1}$ and also reveal widespread overlap between the red and blue high veloc-

ity tails of the emitting gas distribution. Given the potential observational bias of preferentially selecting high redshift QSOs residing in galaxies with approximately face-on orientations (Ho 2007; Narayanan et al. 2008), it appears therefore not unlikely that the outflow in J1148+5152 is indeed bipolar and propagating along the line-of-sight. Note that this means that the actual distance to the spatially extended gas is larger by probably about a least a factor two than the observed projected distances. Note further, that out of our six resimulations, we have picked the one with the most symmetric bipolar outflow. In most simulations in our sample, the outflows show complex geometries resulting in asymmetric or unipolar velocity distributions of the cold gas even for lines-of-sight along the main axis of the outflow.

In Fig. 3, we project the mass of cold metal-enriched material within a slab of thickness 500 kpc along the outflow axis. The image was smoothed with a Gaussian filter with FWHM of 6.7 kpc to match the resolution obtained by Cicone et al. (2015). The distribution of cold outflowing material strongly resembles the irregular morphology of the [CII] image of Cicone et al. (2015) (see their Fig. 3). The projected spatial scale of 20 – 30 kpc of the cold metal-enriched gas is also consistent with their reported value of $\approx 30 \text{ kpc}$. As in Fig. 3 of Cicone et al. (2015), we selected six regions in the QSO vicinity and extracted ‘spectra’ showing the mass of metal-enriched cold gas as a function of line-of-sight velocity. Fast red- and blue-shifted outflowing cold gas is traced by symmetric features in velocity space, e.g. regions α , γ , δ , ϵ , ζ , existing throughout the image over spa-

tial scales of a few tens of kpc. Some of the regions (e.g. β) are instead mainly characterised by a narrow component tracing ‘quiescent’ cold gas, with a velocity width that varies from region to region. We emphasise that as in Cicone et al. (2015), such a narrow component is also spatially extended over a scale of ≈ 30 kpc, but its velocity width is somewhat broader in our simulations. The spectra in Fig. 2 show that spatially extended ‘quiescent’ gas is a common feature of every simulation, including that with no feedback. The narrow component traces gas assembling in the QSO host halo, moving at large angles with respect to the line-of-sight. Part of this gas is in the filaments feeding the halo and part is outflowing (in the simulations with feedback). Unfortunately, the moderate signal-to-noise of Cicone et al. (2015) precludes us from concluding whether the more continuous appearance of the observed spectra is due to observational noise or due to a more complex velocity distribution of cold material than captured by our simulations.

4 DISCUSSION & CONCLUSIONS

Observations of the spatial distribution and kinematics of cold gas surrounding bright high-redshift QSOs provide a remarkable opportunity to probe at the same time the environment of these enigmatic objects and the physical mechanism responsible for AGN feedback. Our simulations show that large velocity widths by themselves are not necessarily an indicator of strong outflows. The rather massive haloes expected to host these bright QSOs develop sufficiently deep potential wells that gravitational motions alone can result in velocity widths as large as $\approx 2000 \text{ km s}^{-1}$ for gas at the centre of the host galaxy.

Much more constraining are therefore the observations of such velocity widths in spatially extended gas reaching out to projected distances $\gtrsim 30$ kpc from the QSO. We have shown here that radiative cooling of the hot shocked outflowing material can account for the formation of entrained cold gas in both supernovae- and AGN-driven outflows at such distances. The large observed velocity at projected distances of $\gtrsim 30$ kpc (Maiolino et al. 2012; Cicone et al. 2015) however require a combination of both. In the absence of supernovae feedback, the AGN-driven outflows that preferentially expand into the voids encounter gas of too low density and metallicity for sufficient cooling to take place. Supernovae-driven outflows pre-enrich the circum/inter-galactic medium with metals and fill it with higher density clumps. If these are overrun by the fast hot AGN outflow, the cooling time of the shocked hot gas significantly decreases, resulting in more vigorous cold and relatively dense outflows. The fastest outflow velocities ($\gtrsim 1400 \text{ km s}^{-1}$) and highest outflow rates of cold gas therefore occur when supernovae- and AGN-driven outflows work in tandem. Strong further clues about the nature of the cold outflows may thereby come from the astonishing blue/red symmetry of the velocity width distribution of the observed spatially extended gas in Cicone et al. (2015). In our simulations, this not only requires a rather special orientation of the line-of-sight, but also a highly symmetric (bipolar) outflow. As we have shown, such highly symmetric outflows occur in our simulations, but this is by no means the generic configuration of the simulated outflows. Characterising larger samples of spatially extended outflows of

cold gas (as well as the strong selection effects of the observed samples) should thus provide valuable information on the environment of bright high-redshift QSOs as well as the physical mechanism driving the outflow.

5 ACKNOWLEDGMENTS

We thank the referee for a helpful report and are grateful to Claudia Cicone, Roberto Maiolino and Sergei Nayakshin for many discussions and helpful suggestions. All simulations used for this study were performed on the Darwin HPC Supercomputer based at the University of Cambridge, UK as part of the DiRAC supercomputing facility. TC acknowledges an STFC studentship and MGH and TC acknowledge support by ERC ADVANCED Grant 320596 ‘The Emergence of Structure during the epoch of Reionization’.

REFERENCES

- Aalto S., Muller S., Sakamoto K., Gallagher J. S., Martín S., Costagliola F., 2012, *A&A*, 546, A68
 Bertoldi F., Carilli C. L., Cox P., Fan X., Strauss M. A., Beelen A., Omont A., Zylka R., 2003, *A&A*, 406, L55
 Bower R. G., Benson A. J., Malbon R., Helly J. C., Frenk C. S., Baugh C. M., Cole S., Lacey C. G., 2006, *MNRAS*, 370, 645
 Cicone C. et al., 2015, *A&A*, 574, A14
 Cicone C. et al., 2014a, *A&A*, 562, A21
 Costa T., Sijacki D., Haehnelt M. G., 2014b, *MNRAS*, 444, 2355
 Costa T., Sijacki D., Trenti M., Haehnelt M. G., 2014a, *MNRAS*, 439, 2146
 Croton D. J. et al., 2006, *MNRAS*, 365, 11
 De Rosa G. et al., 2014, *ApJ*, 790, 145
 Dubois Y., Gavazzi R., Peirani S., Silk J., 2013, *MNRAS*, 433, 3297
 Fabian A. C., 2012, *ARA&A*, 50, 455
 Fan X. et al., 2001, *AJ*, 122, 2833
 Faucher-Giguère C.-A., Lidz A., Zaldarriaga M., Hernquist L., 2009, *ApJ*, 703, 1416
 Faucher-Giguère C.-A., Quataert E., 2012, *MNRAS*, 425, 605
 Genzel R. et al., 2014, *ApJ*, 796, 7
 Haehnelt M. G., Natarajan P., Rees M. J., 1998, *MNRAS*, 300, 817
 Ho L. C., 2007, *ApJ*, 669, 821
 Katz N., Weinberg D. H., Hernquist L., 1996, *ApJS*, 105, 19
 King A., 2003, *ApJ*, 596, L27
 Lynden-Bell D., 1969, *Nature*, 223, 690
 Maiolino R. et al., 2012, *MNRAS*, 425, L66
 McCourt M., O’Leary R. M., Madigan A.-M., Quataert E., 2014, *MNRAS* submitted, arXiv:1409.6719
 Mortlock D. J. et al., 2011, *Nature*, 474, 616
 Narayanan D. et al., 2008, *ApJS*, 174, 13
 Nayakshin S., 2014, *MNRAS*, 437, 2404
 Rees M. J., 1984, *ARA&A*, 22, 471
 Scannapieco E., Oh S. P., 2004, *ApJ*, 608, 62
 Sijacki D., Springel V., Haehnelt M. G., 2009, *MNRAS*, 400, 100

- Sijacki D., Vogelsberger M., Genel S., Springel V., Torrey P., Snyder G., Nelson D., Hernquist L., 2014, MNRAS submitted, arXiv: 1408.6842
- Silk J., Rees M. J., 1998, A&A, 331, L1
- Springel V., 2010, MNRAS, 401, 791
- Springel V., Di Matteo T., Hernquist L., 2005b, MNRAS, 361, 776
- Springel V., Hernquist L., 2003, MNRAS, 339, 289
- Springel V. et al., 2005a, Nature, 435, 629
- Sturm E. et al., 2011, ApJ, 733, L16
- Vogelsberger M., Genel S., Sijacki D., Torrey P., Springel V., Hernquist L., 2013, MNRAS, 436, 3031
- Willott C. J. et al., 2007, AJ, 134, 2435
- Zubovas K., King A. R., 2014, MNRAS, 439, 400
- Zubovas K., Nayakshin S., 2012, MNRAS, 424, 666